Nonadiabatic Hydrogen Tunneling Dynamics for Multiple Proton Transfer Processes with Generalized Nuclear-Electronic Orbital Multistate Density Functional Theory

Joseph A. Dickinson[†] and Sharon Hammes-Schiffer[*,†,‡]

[†]*Department of Chemistry, Yale University, New Haven, Connecticut 06520, USA*

[‡]*Department of Chemistry, Princeton University, Princeton, New Jersey 08544, USA*

E-mail: shs566@princeton.edu

Abstract

Proton transfer and hydrogen tunneling play key roles in many processes of chemical and biological importance. The generalized nuclear-electronic orbital multistate density functional theory (NEO-MSDFT) method was developed in order to capture hydrogen tunneling effects in systems involving the transfer and tunneling of one or more protons. The generalized NEO-MSDFT method treats the transferring protons quantum mechanically on the same level as the electrons and obtains the delocalized vibronic states associated with hydrogen tunneling by mixing localized NEO-DFT states in a nonorthogonal configuration interaction scheme. Herein, we present the derivation and implementation of analytical gradients for the generalized NEO-MSDFT vibronic state energies and the nonadiabatic coupling vectors between these vibronic states. We use this methodology to perform adiabatic and nonadiabatic dynamics simulations of the double proton transfer reactions in the formic acid dimer and the heterodimer of formamidine and formic acid. The generalized NEO-MSDFT method is shown to capture the strongly coupled synchronous or asynchronous tunneling of the two protons in these processes. Inclusion of vibronically nonadiabatic effects is found to significantly impact the double proton transfer dynamics. This work lays the foundation for a variety of nonadiabatic dynamics simulations of multiple proton transfer systems, such as proton relays and hydrogen-bonding networks.

1. Introduction

Proton transfer and hydrogen tunneling are central to many processes of chemical and biological interest,[1–4] including photosynthesis[5] and enzymatic activity.[6,7] Capturing hydrogen tunneling effects is challenging due to the need to account for the delocalization of the tunneling proton(s). The nuclear-electronic orbital (NEO) method provides an elegant framework in which this behavior can be captured directly within quantum chemical calculations. The NEO method is a multicomponent quantum chemistry approach in which both the electrons and select nuclei, usually protons, are quantized and treated with molecular orbital techniques.[8,9] This method incorporates the nuclear quantum effects of the quantized protons, such as zero-point energy and nuclear delocalization, into quantum chemical calculations. The NEO method still invokes the Born-Oppenheimer separation between the quantum and classical subsystems, but the quantum subsystem is composed of both the electrons and the quantized protons, and the classical subsystem is composed of the other, typically heavier, nuclei. Therefore, in trajectory-based NEO quantum dynamics methods,[10,11] the classical nuclei move on vibronic surfaces instead of conventional Born-Oppenheimer electronic surfaces. These vibronic surfaces inherently include contributions from the zero-point energy and nuclear delocalization of the quantized protons.

Many methods based on both wave function theory[8,9,12,13] and density functional theory (DFT)[14–17] have been developed within the NEO framework. NEO-DFT has proven to be particularly useful in simulating proton transfer dynamics due to its balance between computational cost and accuracy.[10,18–20] An important aspect of NEO-DFT is the incorporation of electron-proton correlation (epc) effects via the epc functionals.[10,15,16] Real-time NEO time-dependent DFT (RT-NEO-TDDFT) methods have been applied to gas phase proton transfer systems,[18,20] as well as polaritonic,[21] plasmonic,[22,23] and condensed phase systems.[24] However, the description of hydrogen tunneling systems, where the vibrational wave function of the tunneling proton must delocalize over both wells of a symmetric or nearly symmetric double-well potential,[25–27] is challenging within the NEO framework. In NEO-DFT, the proton densities tend to localize on one side of a hydrogen tunneling system, corresponding to localization in one well of a symmetric double-well potential, leading to incorrect, symmetry-broken solutions.[9,28,29] This localization is mainly due to the lack

of static electron-proton correlation in NEO-DFT, which uses a single product of electronic and protonic Slater determinants as the reference, although dynamical correlation could also play a role.

To properly describe hydrogen tunneling systems within the NEO-DFT framework, we developed the nuclear-electronic orbital multistate density functional theory (NEO-MSDFT) method.[30] Similar to the conventional MSDFT method devised by Gao and coworkers,[31–34] the delocalized vibronic states characteristic of hydrogen tunneling systems are obtained by linearly combining localized NEO-DFT states in a nonorthogonal configuration interaction (NOCI)[35,36] scheme. This strategy directly incorporates both static electron-proton correlation (via the NOCI expansion) and dynamical electron-proton correlation (via the epc functional) into the resulting adiabatic NEO-MSDFT vibronic states. Our previous studies showed that NEO-MSDFT calculations with two localized NEO-DFT states in the NOCI expansion produces bilobal proton densities and accurate hydrogen tunneling splittings for a variety of hydrogen tunneling systems with one quantum proton.[30] Moreover, our generalized NEO-MSDFT method,[37] which allows for an arbitrary number of localized NEO-DFT states in the NOCI expansion, was shown to produce bilobal proton densities and accurate hydrogen tunneling splittings for systems involving multiple proton transfers.

In the conventional picture of hydrogen tunneling, the vibrational wave function of the tunneling proton delocalizes over both wells of a double-well potential when the two minima become degenerate or near-degenerate due to changes in the molecular and/or condensed phase environment. During adiabatic dynamics, where the proton remains in its vibrational ground state, the proton tunnels from the donor well to the acceptor well if the proton potential starts with the donor well lower in energy and ends with the acceptor well lower in energy, passing through a symmetric or nearly symmetric proton potential (left to right in top row of Figure 1). However, nonadiabatic effects among the proton vibrational states can inhibit this tunneling from the donor well to the acceptor well[38] and must be taken into account for an accurate description of hydrogen tunneling dynamics.

In the context of NEO-MSDFT, the nonadiabatic effects between the ground and first excited vibronic NEO-MSDFT states must be considered in the description of hydrogen tunneling. Nonadiabatic dynamics methods,[39–44] such as Ehrenfest[45] and surface hopping dynamics,[38,46,47] can be used to incorporate such effects in hydrogen tunneling simulations. In previous studies, we derived and implemented analytical gradients of the NEO-MSDFT vibronic state energies with respect to the

classical nuclear coordinates,[48] as well as the nonadiabatic coupling vectors between these vibronic states, and investigated the nonadiabatic dynamics of hydrogen tunneling in the intramolecular proton transfer of malonaldehyde.[11] However, the methods employed to calculate these analytical gradients and nonadiabatic coupling vectors were specific to systems with only a single quantum proton and two localized NEO-DFT states.

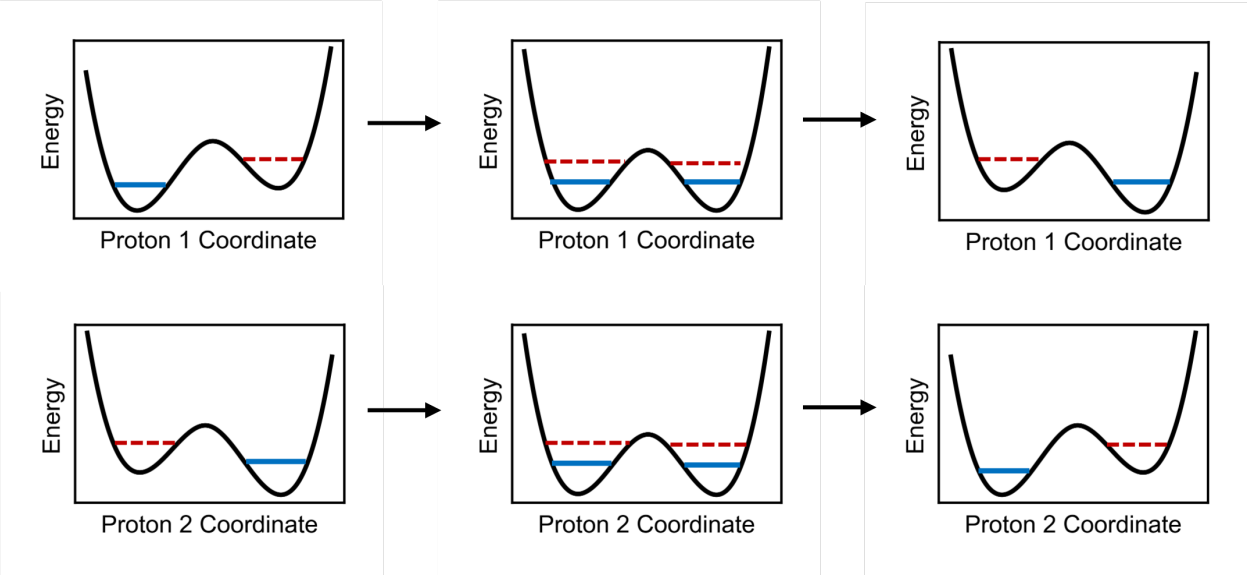

Figure 1. Schematic of double-well proton potentials for the double proton transfer process corresponding to a system such as the formic acid dimer (FAD) or formamidine-formic acid heterodimer (FFAH) shown in Scheme 1. For the first (second) proton, the donor well is on the left (right), and the acceptor well is on the right (left). The ground and first excited proton vibrational states are represented by a solid blue line and a dashed red line, respectively. Due to fluctuations in the molecular structure and/or condensed phase environment, the potentials evolve from being asymmetric (left panels) to symmetric (middle panels) to asymmetric (right panels). The proton vibrational wave functions are localized in one well for the asymmetric proton potentials but are delocalized over both wells for the symmetric proton potential.

Herein, we present a general approach for computing the analytical gradients of the NEO-MSDFT vibronic state energies and the nonadiabatic coupling vectors between these vibronic states. This approach is amenable to the generalized NEO-MSDFT method, thus allowing for the simulation of processes involving multiple proton transfer reactions. To demonstrate the capabilities of the generalized NEO-MSDFT method and the new scheme for computing analytical gradients and nonadiabatic coupling vectors, we performed nonadiabatic dynamics simulations of the intermolecular double proton transfer reactions of the formic acid dimer (FAD)[49–53] and the formamidine-formic

acid heterodimer (FFAH),[54–56] as shown in Scheme 1. These simulations showcase the underlying physical principles of these types of double proton transfer reactions. In particular, these simulations capture the correlated tunneling behavior of the two protons in a manner shown schematically in Figure 1. We emphasize that these two dimeric systems are used to illustrate the capabilities of the NEO-MSDFT approach, and the simulations are not intended to be a comprehensive study of the dynamics or to be comparable to experiments.

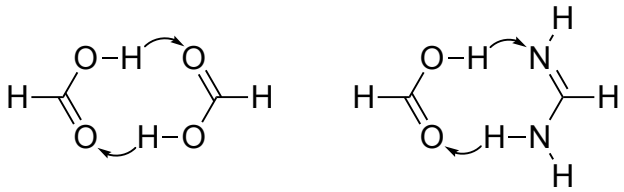

Scheme 1. Double proton transfer mechanisms with arrows pointing in the direction of proton transfer.

This paper is organized as follows. Section 2 provides an overview of the generalized NEO-MSDFT method, presents the new methodology to compute the analytical gradients and nonadiabatic coupling vectors for NEO-MSDFT vibronic states, and explains how these methods are combined with adiabatic, Ehrenfest, and surface hopping dynamics. Section 3 provides the computational details of the simulated double proton transfer reactions. Section 4 gives the results of the dynamics simulations of the two dimeric systems, and Section 5 summarizes this work and outlines future directions.

2. Theory and Methods

2.1. Overview of the Generalized NEO-MSDFT Method

In this subsection, we provide a summary of the generalized NEO-MSDFT method for multiple proton transfer systems. Consider a system with N transferring protons, each subject to a double-well potential in the conventional Born-Oppenheimer picture. Quantizing each of these protons within the NEO framework allows the construction of 2^N localized NEO-DFT states, one for each combination of the quantized protons being localized in their donor or acceptor wells. In NEO-

MSDFT, we first solve for all NEO-DFT states $\{|\tilde{\Psi}_0\rangle, |\tilde{\Psi}_1\rangle, \ldots |\tilde{\Psi}_n\rangle\}$, where $n = 2^N - 1$ and each NEO-DFT state $|\tilde{\Psi}_i\rangle$ is the product of an electronic and protonic Kohn-Sham determinant. These NEO-DFT states are then used as a diabatic basis with which to expand the set of adiabatic NEO-MSDFT states $\{|\Psi_0\rangle, |\Psi_1\rangle, \ldots |\Psi_n\rangle\}$:

$$\begin{aligned}
|\Psi_0\rangle &= D_0^0|\tilde{\Psi}_0\rangle + D_1^0|\tilde{\Psi}_1\rangle + \cdots + D_n^0|\tilde{\Psi}_n\rangle \\
|\Psi_1\rangle &= D_0^1|\tilde{\Psi}_0\rangle + D_1^1|\tilde{\Psi}_1\rangle + \cdots + D_n^1|\tilde{\Psi}_n\rangle \\
&\vdots \qquad\qquad \vdots \qquad\qquad \vdots \\
|\Psi_n\rangle &= D_0^n|\tilde{\Psi}_0\rangle + D_1^n|\tilde{\Psi}_1\rangle + \cdots + D_n^n|\tilde{\Psi}_n\rangle
\end{aligned} \tag{1}$$

In practice, all 2^N possible diabatic NEO-DFT states do not need to be included for an N-proton transfer system, but here we include all diabatic states for the purpose of providing the working equations for the method. The coefficients in Eq. (1) are found by solving the $2^N \times 2^N$ generalized matrix eigenvalue problem

$$\mathbf{HD} = \mathbf{SDE} \tag{2}$$

The overlap matrix $\mathbf{S}$ contains the overlaps between the localized diabatic states

$$\mathbf{S} = \begin{bmatrix} S_{00} & S_{01} & \cdots & S_{0n} \\ S_{10} & S_{11} & \cdots & S_{1n} \\ \vdots & \vdots & \ddots & \vdots \\ S_{n0} & S_{n1} & \cdots & S_{nn} \end{bmatrix} = \begin{bmatrix} 1 & \langle\tilde{\Psi}_0|\tilde{\Psi}_1\rangle & \cdots & \langle\tilde{\Psi}_0|\tilde{\Psi}_n\rangle \\ \langle\tilde{\Psi}_1|\tilde{\Psi}_0\rangle & 1 & \cdots & \langle\tilde{\Psi}_1|\tilde{\Psi}_n\rangle \\ \vdots & \vdots & \ddots & \vdots \\ \langle\tilde{\Psi}_n|\tilde{\Psi}_0\rangle & \langle\tilde{\Psi}_n|\tilde{\Psi}_1\rangle & \cdots & 1 \end{bmatrix} \tag{3}$$

The Hamiltonian matrix $\mathbf{H}$ is given by

$$\mathbf{H} = \begin{bmatrix} H_{00} & H_{01} & \cdots & H_{0n} \\ H_{10} & H_{11} & \cdots & H_{1n} \\ \vdots & \vdots & \ddots & \vdots \\ H_{n0} & H_{n1} & \cdots & H_{nn} \end{bmatrix} \tag{4}$$

The diagonal matrix elements H_{ii} for $i \in \{0, 1, \ldots, n\}$ are simply the NEO-DFT energies of the lo-

calized diabatic states. Specifically, $H_{ii} = E_i^{\text{NEO-DFT}}\left[\rho_i^{\text{e}}, \rho_i^{\text{p}}\right]$, where $\rho_i^{\text{e(p)}}$ is the electronic (protonic) density of the diabatic state $|\tilde{\Psi}_i\rangle$. The off-diagonal matrix elements H_{ij} for $i \neq j$ are computed analogously to the conventional MSDFT method.[32,33,57] These terms are given by

$$H_{ij} = H_{ji} = \langle\tilde{\Psi}_i|\hat{H}_{\text{NEO}}|\tilde{\Psi}_j\rangle + \frac{1}{2}S_{ij}(E_i^{\text{corr}} + E_j^{\text{corr}}) \tag{5}$$

Here $\langle\tilde{\Psi}_i|\hat{H}_{\text{NEO}}|\tilde{\Psi}_j\rangle$ is the energy computed with the NEO Hamiltonian $\hat{H}_{\text{NEO}}$ at the NEO Hartree-Fock (NEO-HF) level with the NEO Kohn-Sham determinants of diabatic states $|\tilde{\Psi}_i\rangle$ and $|\tilde{\Psi}_j\rangle$. Moreover, E_i^{corr} for $i \in \{0, 1, \ldots, n\}$ is the correlation energy for diabatic state $|\tilde{\Psi}_i\rangle$, defined as the difference between the NEO-DFT and NEO-HF energies: $E_i^{\text{corr}} = E_i^{\text{NEO-DFT}}\left[\rho_i^{\text{e}}, \rho_i^{\text{p}}\right] - E_i^{\text{NEO-HF}}\left[\rho_i^{\text{e}}, \rho_i^{\text{p}}\right]$. Note that the matrix elements in Eq. (5) are dependent on the choice of diabatic basis, as is the case for all NOCI problems.[35,36] The physical motivation for the form of these off-diagonal Hamiltonian matrix elements[30] is discussed in Section S2 of the Supporting Information (SI). Additional details on the computation of all matrix elements are provided in Section S1 of the SI.

As discussed in our previous work,[30,37,48] we apply a correction function to the off-diagonal elements of the overlap matrix to account for the limitations of the epc17-2 electron-proton correlation functional.[15,16] This functional produces proton densities that are slightly too localized, leading to off-diagonal overlap matrix elements that are slightly too small. In this scheme, the off-diagonal matrix elements of the $\mathbf{S}$ matrix are replaced as follows:

$$S'_{ij} = \alpha(S_{ij})^{\beta}, \tag{6}$$

where $\alpha = 0.0604$ and $\beta = 0.492$. Typically the corrected overlap is slightly larger than the original overlap to mitigate the effects of the over-localized proton densities obtained with the epc17-2 functional. The two parameters were determined for a simple model system and were subsequently shown to be robust and transferable for the systems studied. Specifically, the NEO-MSDFT method, in conjunction with this corrected overlap matrix, has been shown to produce accurate hydrogen tunneling splittings for a wide range of geometries of five different single quantum proton molecular systems[30] and four different double quantum proton molecular systems.[37]

Analytical gradients of the NEO-MSDFT vibronic state energies have only been derived for the original two-state NEO-MSDFT method,[48] allowing nonadiabatic dynamics simulations of single proton transfer systems[11] but not multiple proton transfer systems that require more than two diabatic vibronic states. The next subsection will present an approach to compute the analytical gradients and nonadiabatic coupling vectors for the generalized NEO-MSDFT method.

2.2. Analytical Gradients and Nonadiabatic Coupling Vectors for Generalized NEO-MSDFT

In this subsection, we present a new generalized algorithm for computing analytical gradients and nonadiabatic coupling vectors for NEO-MSDFT adiabatic vibronic states. In the original two-state NEO-MSDFT method, the NEO-MSDFT energies and their gradients could be expressed analytically as a function of the matrix elements of $\mathbf{H}$ and $\mathbf{S}$, which are 2×2 matrices. However, this is not generally true for Hamiltonian matrices of arbitrary dimensionality. To obtain the analytical gradients of the NEO-MSDFT energies for the generalized case, we need a scheme that is independent of the dimensionality of the NEO-MSDFT Hamiltonian, or equivalently, the number of NEO-DFT diabatic states included in the NOCI expansion of Eq. (1). This subsection presents such a scheme.

We assume that $\nabla_{\mathbf{R}} H_{ij}$ and $\nabla_{\mathbf{R}} S_{ij}$ have been computed for all $i, j \in \{0, 1, \ldots, n\}$. We provide the expressions for these gradients in Section S1 of the SI. We also assume that we have already constructed and solved the NEO-MSDFT eigenvalue problem of Eq (2). Let x_k be some arbitrary nuclear coordinate. Then the gradient of the i-th NEO-MSDFT energy eigenvalue E_i with respect to x_k is given by

$$\frac{\partial E_i}{\partial x_k} = \mathbf{d}_i^{\mathrm{T}} \left(\frac{\partial \mathbf{H}}{\partial x_k} - E_i \frac{\partial \mathbf{S}}{\partial x_k} \right) \mathbf{d}_i \tag{7}$$

where $\mathbf{d}_i$ is the i-th eigenvector satisfying $\mathbf{d}_i^{\mathrm{T}} \mathbf{S} \mathbf{d}_i = 1$ (i.e., the vector $\mathbf{d}_i$ is a column of $\mathbf{D}$ with

elements D_q^i for $q = 0, 1, \ldots n$). The matrix derivatives are of the form

$$\frac{\partial \mathbf{H}}{\partial x_k} = \begin{bmatrix} \frac{\partial E_0^{\text{NEO-DFT}}}{\partial x_k} & \frac{\partial H_{01}}{\partial x_k} & \cdots & \frac{\partial H_{0n}}{\partial x_k} \\ \frac{\partial H_{10}}{\partial x_k} & \frac{\partial E_1^{\text{NEO-DFT}}}{\partial x_k} & \cdots & \frac{\partial H_{1n}}{\partial x_k} \\ \vdots & \vdots & \ddots & \vdots \\ \frac{\partial H_{n0}}{\partial x_k} & \frac{\partial H_{n1}}{\partial x_k} & \cdots & \frac{\partial E_n^{\text{NEO-DFT}}}{\partial x_k} \end{bmatrix}, \quad \frac{\partial \mathbf{S}}{\partial x_k} = \begin{bmatrix} 0 & \frac{\partial S_{01}}{\partial x_k} & \cdots & \frac{\partial S_{0n}}{\partial x_k} \\ \frac{\partial S_{10}}{\partial x_k} & 0 & \cdots & \frac{\partial S_{1n}}{\partial x_k} \\ \vdots & \vdots & \ddots & \vdots \\ \frac{\partial S_{n0}}{\partial x_k} & \frac{\partial S_{n1}}{\partial x_k} & \cdots & 0 \end{bmatrix} \tag{8}$$

A derivation of Eq. (7) is given in Section S3 of the SI, along with a more general discussion about computing derivatives for generalized eigenvalue problems. Thus, the problem of solving for the gradient vector $\nabla_{\mathbf{R}} E_i$ reduces to applying Eq. (7) for each nuclear coordinate x_k.

To perform nonadiabatic dynamics simulations, we must also compute the nonadiabatic coupling vector between two NEO-MSDFT vibronic states, i.e., $\langle \Psi_i | \nabla_{\mathbf{R}} \Psi_j \rangle$. Inserting the expansion of Eq. (1) into $\langle \Psi_i | \nabla_{\mathbf{R}} \Psi_j \rangle$ leads to

$$\begin{aligned} \langle \Psi_i | \nabla_{\mathbf{R}} \Psi_j \rangle &= \left\langle \sum_q D_q^i \tilde{\Psi}_q \middle| \nabla_{\mathbf{R}} \sum_r D_r^j \tilde{\Psi}_r \right\rangle \\ &= \sum_{qr} \left[D_q^i \left(\nabla_{\mathbf{R}} D_r^j \right) S_{qr} + D_q^i D_r^j \langle \tilde{\Psi}_q | \nabla_{\mathbf{R}} \tilde{\Psi}_r \rangle \right] \end{aligned} \tag{9}$$

Thus, the nonadiabatic coupling vector $\langle \Psi_i | \nabla_{\mathbf{R}} \Psi_j \rangle$ depends on the gradients of the expansion coefficients of Eq. (1) as well as the nonadiabatic coupling vector between diabatic NEO-DFT states of the form $\langle \tilde{\Psi}_q | \nabla_{\mathbf{R}} \tilde{\Psi}_r \rangle$. The $\nabla_{\mathbf{R}} D_r^j$ term in Eq. (9) is the gradient vector of the expansion coefficient of diabatic state $|\tilde{\Psi}_r\rangle$ for the adiabatic state $|\Psi_j\rangle$. The gradient of the associated j-th eigenvector $\mathbf{d}_j$ with respect to nuclear coordinate x_k can be computed according to

$$\frac{\partial \mathbf{d}_j}{\partial x_k} = -\mathbf{D} \left(\mathbf{E} - E_j \mathbf{I} \right)^+ \mathbf{D}^{\mathrm{T}} \left(\frac{\partial \mathbf{H}}{\partial x_k} - E_j \frac{\partial \mathbf{S}}{\partial x_k} \right) \mathbf{d}_j - \frac{1}{2} \left(\mathbf{d}_j^{\mathrm{T}} \frac{\partial \mathbf{S}}{\partial x_k} \mathbf{d}_j \right) \mathbf{d}_j \tag{10}$$

where the + superscript denotes the Moore-Penrose pseudoinverse. Thus, the problem of solving for $\nabla_{\mathbf{R}} D_r^j$ reduces to applying Eq. (10) for each nuclear coordinate x_k and taking the r-th element of the resultant vector. More details are provided in Section Eq. S3 of the SI. The expression for the $\langle \tilde{\Psi}_i | \nabla_{\mathbf{R}} \tilde{\Psi}_j \rangle$ terms in Eq. (9) is more involved and is provided in Section S4 of the SI.

In conventional electronic structure theory, electron-translation factors [58,59] have been introduced

to ensure translational invariance of the nonadiabatic coupling vectors. These electron-translation factors are often negligible but have been shown to be important for some systems. In the NEO framework, electron-proton translation factors may be required for this purpose. Based on previous studies with conventional electronic structure methods Eq.[59] and the use of fixed proton basis function centers herein, we do not anticipate that such multicomponent translation factors would significantly impact the nonadiabatic dynamics simulations presented in this work.

2.3. Adiabatic and Nonadiabatic Dynamics on NEO-MSDFT Vibronic Surfaces

This subsection presents the theory underlying adiabatic, Ehrenfest, and surface hopping dynamics within the NEO-MSDFT framework. Note that the adiabatic NEO-MSDFT vibronic states $\{|\Psi_0\rangle, |\Psi_1\rangle, \ldots |\Psi_n\rangle\}$ depend explicitly on the positions of the electrons $\mathbf{r}^{\mathrm{e}}$ and quantum protons $\mathbf{r}^{\mathrm{p}}$ and depend parametrically on the positions of the classical nuclei $\mathbf{R}$.

In adiabatic dynamics, the classical nuclei move on the NEO-MSDFT ground vibronic surface according to Newton's equations of motion. In this case,

$$M_I \ddot{\mathbf{R}}_I(t) = -\nabla_{\mathbf{R}_I} \langle \Psi_0(\mathbf{r}^{\mathrm{e}}, \mathbf{r}^{\mathrm{p}}; \mathbf{R}) | \hat{H}_{\mathrm{NEO}} | \Psi_0(\mathbf{r}^{\mathrm{e}}, \mathbf{r}^{\mathrm{p}}; \mathbf{R}) \rangle = -\nabla_{\mathbf{R}_I} E_0 \tag{11}$$

where M_I and $\mathbf{R}_I$ are the mass and position coordinate, respectively, of the I-th classical nucleus.

In both Ehrenfest and surface hopping dynamics, the total time-dependent vibronic wave function $|\Phi(\mathbf{r}^{\mathrm{e}}, \mathbf{r}^{\mathrm{p}}, t; \mathbf{R})\rangle$ is expanded as a linear combination of the adiabatic NEO-MSDFT vibronic states with time-dependent coefficients

$$|\Phi(\mathbf{r}^{\mathrm{e}}, \mathbf{r}^{\mathrm{p}}, t; \mathbf{R})\rangle = \sum_k C_k(t) |\Psi_k(\mathbf{r}^{\mathrm{e}}, \mathbf{r}^{\mathrm{p}}; \mathbf{R})\rangle \tag{12}$$

where the sum in Eq. (12) is over all the adiabatic vibronic states of interest. In practice, this summation is often limited to the ground and first excited NEO-MSDFT vibronic states because the current implementation of NEO-MSDFT does not include bending modes in the diabatic basis and therefore does not provide a complete set of higher-lying vibrational states.[37] In principle, the diabatic basis can be expanded to include such modes, but for most purposes, the two lowest-

lying vibronic states are sufficient to describe hydrogen tunneling. Thus, although the generalized NEO-MSDFT method allows for the inclusion of an arbitrary number of localized NEO-DFT diabatic states in the NOCI expansion of Eq. (1), often only the ground and first excited adiabatic NEO-MSDFT vibronic states are relevant for describing nonadiabatic hydrogen tunneling dynamics. However, the analytical expressions for the energies, gradients, and nonadiabatic coupling vectors, as well as the dynamics methods discussed in this section, are applicable for an arbitrary number of adiabatic NEO-MSDFT vibronic states.

The total time-dependent vibronic wave function $|\Phi(\mathbf{r}^{\mathrm{e}}, \mathbf{r}^{\mathrm{p}}, t; \mathbf{R})\rangle$ obeys the time-dependent Schrödinger equation

$$i\hbar \frac{\partial}{\partial t} |\Phi(\mathbf{r}^{\mathrm{e}}, \mathbf{r}^{\mathrm{p}}, t; \mathbf{R})\rangle = \hat{H}_{\mathrm{NEO}} |\Phi(\mathbf{r}^{\mathrm{e}}, \mathbf{r}^{\mathrm{p}}, t; \mathbf{R})\rangle \tag{13}$$

Substituting the expansion in Eq. (12) into Eq. (13) leads to a coupled set of differential equations describing the time evolution of the coefficients in Eq. (12):

$$\dot{C}_j(t) = -\sum_k C_k(t) \left(\left\langle \Psi_j(\mathbf{r}^{\mathrm{e}}, \mathbf{r}^{\mathrm{p}}; \mathbf{R}) \middle| \frac{\partial}{\partial t} \Psi_k(\mathbf{r}^{\mathrm{e}}, \mathbf{r}^{\mathrm{p}}; \mathbf{R}) \right\rangle + \frac{i}{\hbar} E_k \delta_{jk} \right) \tag{14}$$

where the time-dependent nonadiabatic coupling element between adiabatic states $|\Psi_j(\mathbf{r}^{\mathrm{e}}, \mathbf{r}^{\mathrm{p}}; \mathbf{R})\rangle$ and $|\Psi_k(\mathbf{r}^{\mathrm{e}}, \mathbf{r}^{\mathrm{p}}; \mathbf{R})\rangle$ can be expressed as

$$\left\langle \Psi_j(\mathbf{r}^{\mathrm{e}}, \mathbf{r}^{\mathrm{p}}; \mathbf{R}) \middle| \frac{\partial}{\partial t} \Psi_k(\mathbf{r}^{\mathrm{e}}, \mathbf{r}^{\mathrm{p}}; \mathbf{R}) \right\rangle = \langle \Psi_j(\mathbf{r}^{\mathrm{e}}, \mathbf{r}^{\mathrm{p}}; \mathbf{R}) | \nabla_{\mathbf{R}} \Psi_k(\mathbf{r}^{\mathrm{e}}, \mathbf{r}^{\mathrm{p}}; \mathbf{R}) \rangle \cdot \mathbf{v} \tag{15}$$

Here $\mathbf{d}_{jk} \equiv \langle \Psi_j(\mathbf{r}^{\mathrm{e}}, \mathbf{r}^{\mathrm{p}}; \mathbf{R}) | \nabla_{\mathbf{R}} \Psi_k(\mathbf{r}^{\mathrm{e}}, \mathbf{r}^{\mathrm{p}}; \mathbf{R}) \rangle$ is the nonadiabatic coupling vector between the specified vibronic states, as introduced in Eq. (9), and $\mathbf{v}$ is the vector of velocities of the classical nuclei. The nonadiabatic coupling elements can be computed analytically using Eq. (15) together with Eq. (9). However, calculating the nonadiabatic coupling elements numerically is more stable and ensures accuracy even when they increase rapidly over the course of a time step.[60] Section 3 provides details about the calculation of these nonadiabatic coupling terms in our simulations.

Although both Ehrenfest and surface hopping dynamics begin with the same ansatz for the total vibronic wave function (Eq. (12)), they differ in how the nuclear dynamics are propagated. In

Ehrenfest dynamics, the classical nuclei move on an average vibronic surface according to

$$\begin{aligned} M_I \ddot{\mathbf{R}}_I(t) &= -\nabla_{\mathbf{R}_I} \langle \Phi(\mathbf{r}^{\mathrm{e}}, \mathbf{r}^{\mathrm{p}}, t; \mathbf{R}) | \hat{H}_{\mathrm{NEO}} | \Phi(\mathbf{r}^{\mathrm{e}}, \mathbf{r}^{\mathrm{p}}, t; \mathbf{R}) \rangle \\ &= -\sum_{jk} C_j^*(t) C_k(t) \langle \Psi_j(\mathbf{r}^{\mathrm{e}}, \mathbf{r}^{\mathrm{p}}; \mathbf{R}) | \nabla_{\mathbf{R}_I} \hat{H}_{\mathrm{NEO}} | \Psi_k(\mathbf{r}^{\mathrm{e}}, \mathbf{r}^{\mathrm{p}}; \mathbf{R}) \rangle \end{aligned} \tag{16}$$

The diagonal matrix elements of $\nabla_{\mathbf{R}} \hat{H}_{\mathrm{NEO}}$ are the gradients of the diabatic NEO-DFT states, and the off-diagonal matrix elements are related to the nonadiabatic coupling vector as follows:

$$\mathbf{d}_{jk} = \frac{\langle \Psi_j(\mathbf{r}^{\mathrm{e}}, \mathbf{r}^{\mathrm{p}}; \mathbf{R}) | \nabla_{\mathbf{R}} \hat{H}_{\mathrm{NEO}} | \Psi_k(\mathbf{r}^{\mathrm{e}}, \mathbf{r}^{\mathrm{p}}; \mathbf{R}) \rangle}{E_k - E_j} \tag{17}$$

The time-dependent coefficients in Eq. (16) are propagated numerically according to Eq. (14).

In surface hopping dynamics, the nuclear dynamics are propagated on a single adiabatic NEO-MSDFT vibronic surface k according to

$$M_I \ddot{\mathbf{R}}_I(t) = -\nabla_{\mathbf{R}_I} \langle \Psi_k(\mathbf{r}^{\mathrm{e}}, \mathbf{r}^{\mathrm{p}}; \mathbf{R}) | \hat{H}_{\mathrm{NEO}} | \Psi_k(\mathbf{r}^{\mathrm{e}}, \mathbf{r}^{\mathrm{p}}; \mathbf{R}) \rangle = -\nabla_{\mathbf{R}_I} E_k \tag{18}$$

Instantaneous transitions between adiabatic vibronic states can be incorporated through a stochastic algorithm, such as Tully's fewest switches algorithm,[46] based on the time-dependent coefficients obtained by numerically propagating Eq (14). In our simulations, we did not employ a stochastic algorithm to determine when transitions between adiabatic vibronic states would occur. We elaborate on the procedure we used for incorporating nonadiabatic transitions in Section 3. After a transition between adiabatic vibronic states occurs, the velocities of the classical nuclei are scaled, typically in the direction of the nonadiabatic coupling vector, to maintain energy conservation.[38]

3. Computational Details

In this section, we provide the computational details of the nonadiabatic dynamics simulations we conducted of the double proton transfer reactions in the FAD and the FFAH systems. The FAD exhibits a concerted double proton transfer and lacks a stable intermediate along the minimum energy path connecting the two degenerate minima through the transition state on its ground-

state electronic potential energy surface. Therefore, in our FAD simulations, only the two *trans* NEO-DFT diabatic vibronic states were included in the NOCI expansion of Eq. (1), as shown in Figure 2A. In contrast to FAD, however, the double proton transfer in FFAH involves the formation of a stable intermediate corresponding to the zwitterionic state, which is a minimum on the ground state electronic potential energy surface. Thus, in addition to the *trans* NEO-DFT diabatic vibronic states, we also included the zwitterionic NEO-DFT diabatic vibronic state in the NOCI expansion, as shown in Figure 2B.

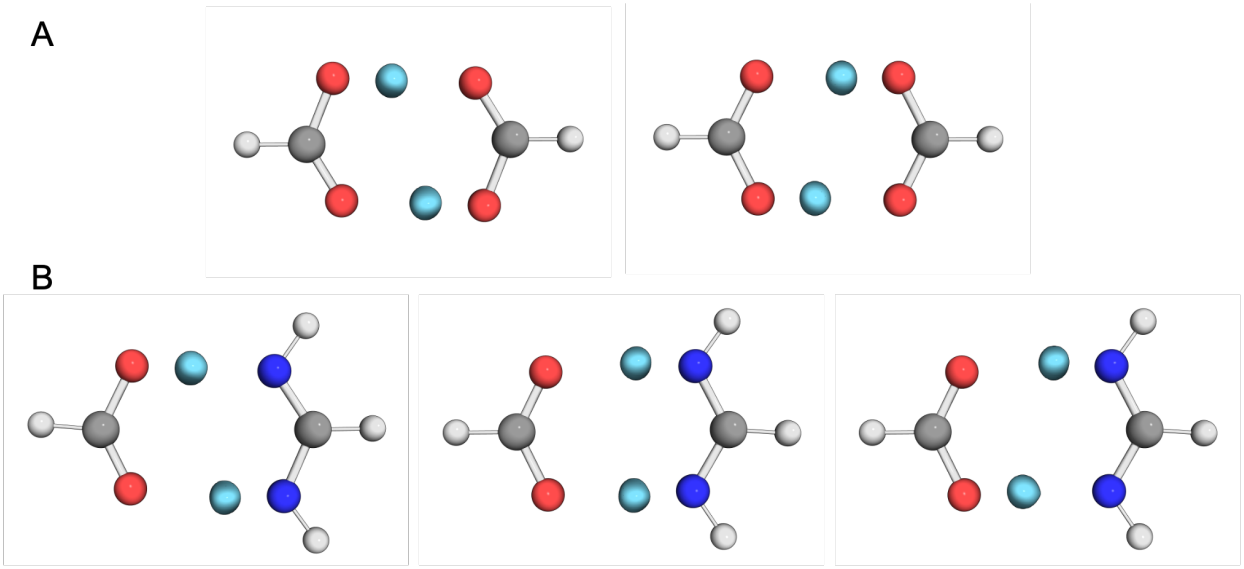

Figure 2. The NEO-DFT diabatic vibronic states included in the NEO-MSDFT simulations of (A) the FAD and (B) the FFAH. For the FAD, we only included the *trans* states of the double proton transfer process. For the FFAH, we also included the zwitterionic intermediate (middle structure in (B)). The proton density of each diabatic state is shown in cyan.

For each system, one adiabatic trajectory, one Ehrenfest trajectory, and one sample surface hopping trajectory were propagated. The computational cost of the current implementation prohibits us from running a converged surface hopping simulation, which would require at least ∼100 trajectories. Only two NEO-MSDFT adiabatic vibronic states were included in the expansion of Eq. (12) for the nonadiabatic trajectories. All FAD trajectories were given the same initial conditions, and all FFAH trajectories were given the same initial conditions. An equilibrium geometry for each system was found, and velocities were initialized to facilitate motion toward an average reactant-product structure for each system. More details on the initialization of these trajectories and how these structures were obtained are given in Section S11 of the SI. Note that on the short

timescales of these trajectories, the classical nuclei move only a small amount but enough to induce double proton transfer.

The generalized NEO-MSDFT method was implemented in a development version of Q-Chem 6.1[61] and is currently available in the latest release version. The nuclear dynamics were propagated using an in-house code interfaced with Q-Chem. A time step of 0.05 fs was used to propagate the classical nuclei for a total of 7.00 fs for each trajectory. To integrate Eq. (14), a fourth-order Runge-Kutta integration technique was employed with a time step of 0.0002 fs. To calculate the time-dependent nonadiabatic coupling elements, we used a generalized version[62] of the norm-preserving interpolation procedure first introduced by Meek and Levine,[60] with more details given in Section S6 of the SI.

The values of these nonadiabatic coupling elements were used to determine when the transitions between adiabatic vibronic states occurred in each of our sample surface hopping trajectories. In both surface hopping trajectories presented, we pre-determined two transitions: one from the ground state to the first excited state, and one back down from the first excited state to the ground state. The first transition was chosen to occur at the time where the nonadiabatic coupling element reached its maximum value along the adiabatic trajectory for each system. The second transition was chosen to occur at the first time step where the nonadiabatic coupling element dropped below 1.5 fs^{-1} after reaching its maximum, which is a large enough nonadiabatic coupling to be associated with a reasonable probability of a transition in a stochastic surface hopping algorithm. At both transitions, the velocities of the classical nuclei were rescaled in the direction of the nonadiabatic coupling vector in order to maintain energy conservation. We emphasize that these choices for incorporating nonadiabatic transitions were simply meant to produce a sample surface hopping trajectory. Obtaining meaningful results for surface hopping dynamics requires the propagation of a large number of trajectories.

In all calculations herein, we used the electronic B3LYP exchange-correlation functional[63,64] and the epc17-2 electron-proton correlation functional,[15,16] along with the cc-pVDZ electronic basis set[65] and the PB4-D protonic basis set.[66] In NEO-MSDFT, each quantum transferring proton is given two protonic basis function centers, where each center is located near the minimum of one of the two wells of the corresponding double-well proton potential. In our previous study of

malonaldehyde,[11] each of these centers was optimized variationally on the appropriate NEO-MSDFT vibronic surface. However, in this work, the positions of these protonic basis function centers were kept fixed because the proton transfer reactions occurred prior to translation or rotation of the system, and the optimization of the centers proved to be the bottleneck of these simulations. Details about the determination of the proton basis function center positions are provided in Section S11 of the SI.

We emphasize that a converged set of fixed proton basis function centers has been shown to provide accurate quantum dynamics and to conserve energy for RT-NEO-TDDFT calculations.[19,20] A disadvantage of this scheme, however, is that the path of the proton must be known to ensure convergence of the basis set. Alternative schemes have been devised to address this issue. For example, the proton basis function center positions can be optimized variationally, as in our previous NEO-MSDFT nonadiabatic dynamics simulations of single proton transfer reactions.[11] The analytical gradients presented herein could be used to optimize the proton basis function center positions at each time step but were kept fixed for the sake of computational efficiency. Alternatively, a traveling proton basis function center scheme[19,20] could potentially be extended for use with NEO-MSDFT. More computationally efficient optimization routines[67–69] may also be used in this regard. However, the qualitative dynamics presented in Section 4 are not impacted by the use of fixed rather than optimized or traveling proton basis function centers.

4. Results and Discussion

4.1. Formic Acid Dimer

First we present an analysis of the FAD trajectories at a qualitative level. A more in-depth discussion of the quantitative results for the FFAH trajectories will be presented below. The time evolution of the proton densities for each of the three FAD trajectories is provided in Figure 3. The double proton transfer reactions for all three of these FAD trajectories are concerted. The quantitative results for the FAD trajectories are provided in Section S7 of the SI.

For the adiabatic trajectory, the system remains in the ground NEO-MSDFT vibronic state for the duration of the trajectory (Figure 3A). The system begins in its initial reactant configuration,

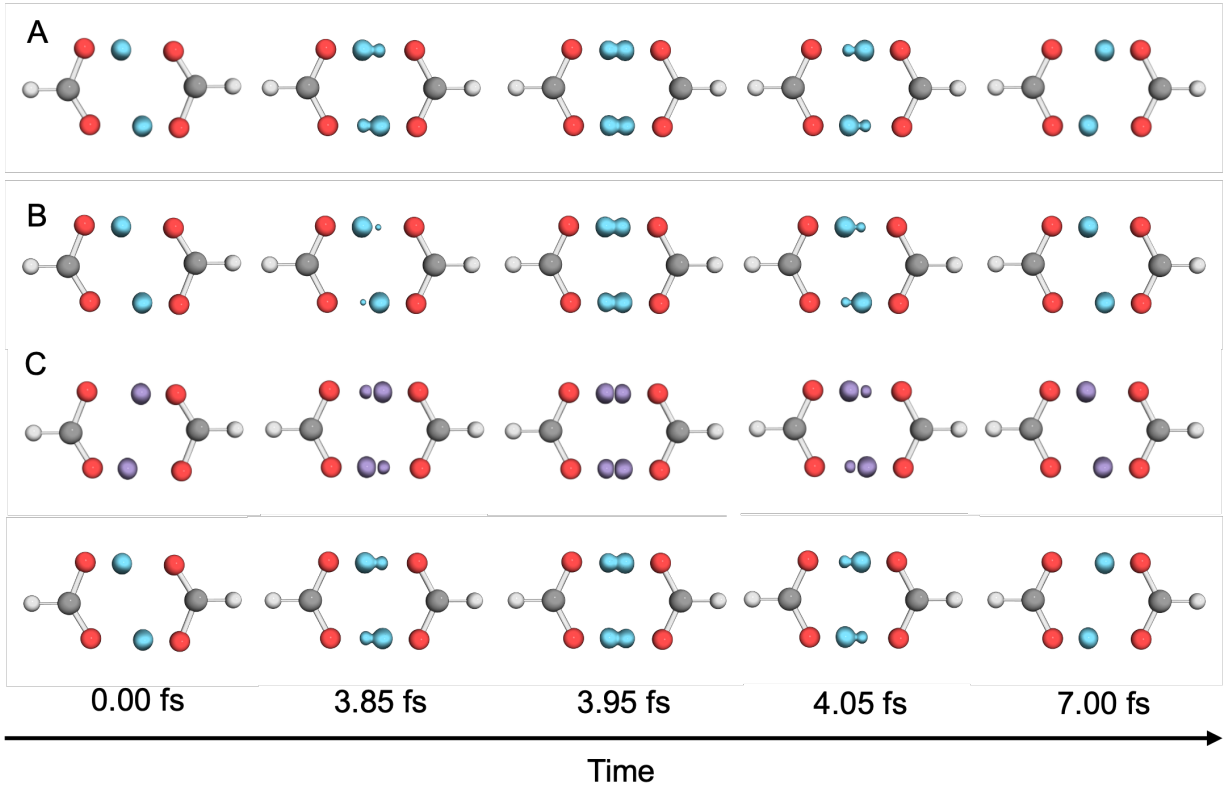

Figure 3. Proton densities along the (A) adiabatic, (B) Ehrenfest, and (C) sample surface hopping trajectories for the FAD. In (A), the proton density for the ground NEO-MSDFT vibronic state is shown in cyan. In (B), the proton density associated with the average NEO-MSDFT vibronic surface is shown in cyan. In (C), the proton densities for the ground and first excited NEO-MSDFT vibronic states are shown in cyan and purple, respectively. For the sample surface hopping trajectory, the system is in the ground vibronic state for all times shown except 3.95 fs, where it is in the first excited vibronic state.

where the quantum protons are localized near their respective oxygen donors on opposite sides of the dimer structure (analogous to the solid blue lines in the left panels of Figure 1). At ∼3.85 fs, the proton densities become delocalized across both wells but are still asymmetric. At 3.95 fs, the system reaches its most symmetric configuration (analogous to the solid blue lines in the middle panels of Figure 1). Then the system continues toward its product state, which is the opposite *trans* structure from which it was initialized (analogous to the solid blue lines in the right panels of Figure 1), completing the double proton transfer process in the FAD.

The purely adiabatic picture of the double proton transfer process is incomplete because it neglects the nonadiabatic effects associated with the first excited vibronic state, and these effects are known to inhibit proton transfer events.[38] We first incorporate these nonadiabatic effects at a mean-field level via Ehrenfest dynamics (Figure 3B). The Ehrenfest trajectory proceeds in exactly the same fashion as the adiabatic trajectory until the nonadiabatic coupling between the ground and first excited NEO-MSDFT vibronic states becomes non-negligible at ∼3.50 fs (Figure S2D). The nonadiabatic coupling in this region causes the proton density on the average NEO-MSDFT vibronic surface to deviate from its adiabatic counterpart at comparable times (i.e., the Ehrenfest proton density is not as delocalized as the adiabatic proton density at 3.85 fs in Figure 3). Similar to the adiabatic trajectory, at ∼3.95 fs, the proton densities delocalize across both wells. However, at this time, the nonadiabatic coupling between the ground and first excited NEO-MSDFT vibronic states increases rapidly, causing the quantum probabilities to switch from $|C_0(t)|^2 = 1$ to $|C_1(t)|^2 = 1$ at ∼ 3.95 fs (Figure S2C). The system then quickly exits this region of strong nonadiabatic coupling, preventing any further evolution of the quantum amplitudes. Therefore, the average NEO-MSDFT vibronic surface dictating the nuclear dynamics is essentially the first excited NEO-MSDFT vibronic state for the remainder of the trajectory. As a result, the proton densities are localized on their donors at the end of the process (analogous to the dashed red lines in the right panels of Figure 1). Thus, the double proton transfer is inhibited when nonadiabatic effects are incorporated at the mean field level for these initial conditions.

Nonadiabatic effects can also be incorporated via a surface hopping procedure, where the classical nuclei evolve on a single adiabatic vibronic state, with stochastic transitions between adiabatic vibronic states incorporated according to an algorithm based on their quantum amplitudes. How-

ever, such an approach would necessitate propagating a large number of trajectories in order to obtain statistically meaningful results. Therefore, as a proof-of-concept, we only propagated one surface hopping trajectory (Figure 3C), where two hops were predetermined to occur, as explained in Section 3. Our FAD surface hopping trajectory proceeds in exactly the same manner as the adiabatic trajectory until it reaches 3.95 fs, the time at which the first hop was predetermined to occur. At this time, the system transitions to the first excited vibronic state, where it remains for 0.10 fs before it transitions back down to the ground vibronic state. For this trajectory, the system did not remain in the first excited vibronic state long enough to produce obvious differences in the proton densities compared to the adiabatic trajectory. As mentioned above, a converged surface hopping simulation would require propagation of a large number of trajectories.

4.2. Formamimide-Formic Acid Heterodimer

The FAD double proton transfer system discussed in the previous subsection involves significant contributions from only two localized NEO-DFT diabatic vibronic states. In contrast, the FFAH system involves significant contributions from three localized NEO-DFT diabatic vibronic states, thus necessitating the generalized algorithm for obtaining analytical gradients and nonadiabatic couplings discussed in Section 2.1. For this system, we present a more detailed analysis of the double proton transfer dynamics.

The double proton transfer of FFAH proceeds via a stepwise mechanism in the conventional Born-Oppenheimer picture. The minimum energy path connecting the two degenerate minima of its ground state electronic potential energy surface exhibits a local minimum corresponding to the zwitterionic state of the heterodimer,[54–56] where both protons are localized on the formamidine side of the dimer structure with positive/negative charges distributed across the formamidine/formic acid monomers, respectively. As shown below, the typical stepwise mechanism of this double proton transfer is recast in the NEO framework as an asynchronous but strongly coupled tunneling of the two protons, where one proton becomes delocalized and bilobal prior to the delocalization of the other proton, but both protons can be delocalized and bilobal simultaneously.

For the adiabatic trajectory, the system begins in the reactant state, where the top proton is localized near the formic acid monomer and the bottom proton is localized near the formamidine

monomer (Figure 4). At ∼3.65 fs, the top proton becomes delocalized and bilobal, while the bottom proton remains localized nears its donor. This process is analogous to the system approaching the zwitterionic state in the conventional Born-Oppenheimer picture. See Figure S4 for a quantitative analysis of how much the zwitterionic state contributes to each adiabatic NEO-MSDFT vibronic state for all FFAH trajectories.

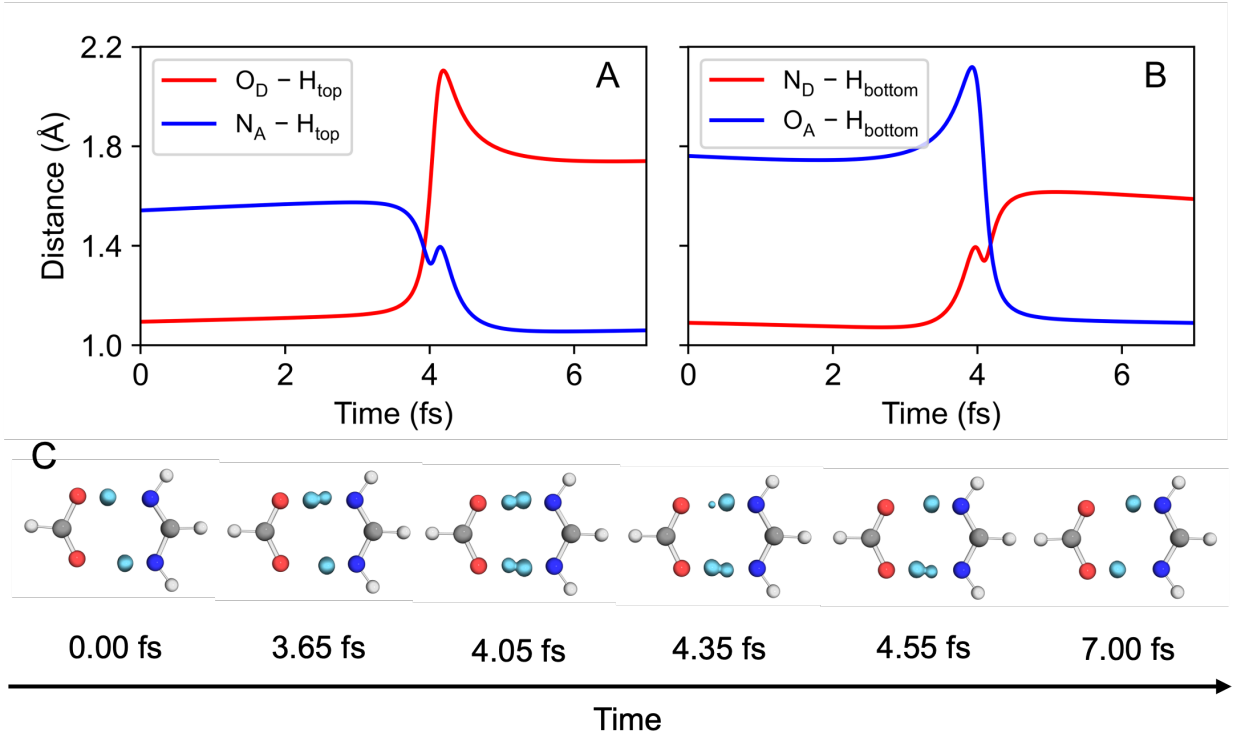

Figure 4. Analysis of the adiabatic trajectory for the FFAH dimer. The distances between the (A) top and (B) bottom proton position expectation values and the corresponding donor (red) and acceptor (blue) for the NEO-MSDFT ground vibronic state are plotted along the trajectory. (C) Proton density of the ground NEO-MSDFT adiabatic vibronic state shown in cyan along the adiabatic trajectory.

At ∼3.90 fs, the proton density of the top proton is delocalized and bilobal, and its expectation value is equidistant from its donor and acceptor. At 4.05 fs, both protons are delocalized and bilobal (solid blue lines in middle panels of Figure 1). Note that around this time, it appears that the protons are moving further away from both their donors and acceptors (slightly after 4 fs in Figure 4A and slightly before 4 fs in 4B). This behavior can be explained in terms of the relative positioning of the protons in the zwitterionic state, which is the dominant diabatic vibronic state in this range. In the *trans* diabatic vibronic states, the expectation values of the two protons

are positioned nearly exactly on their respective donor-acceptor axes, defined as the straight line connecting the donor and acceptor nuclei. In the zwitterionic diabatic vibronic state, however, the expectation values of the protons are no longer close to their donor-acceptor axes and instead pucker outward from the interior of the dimer structure.

After both protons delocalize and the system begins to exit the region dominated by the zwitterionic diabatic vibronic state, the two protons finish their transfers in the order in which they delocalized. The top proton localizes completely on its acceptor at ∼4.55 fs, whereas the bottom proton remains delocalized until a short time later, when it localizes completely on its acceptor. Thus, instead of observing a stepwise mechanism for the double proton transfer, as in the conventional Born-Oppenheimer picture of this process, we observe asynchronous but strongly coupled tunneling of the two protons. First the top proton becomes delocalized and bilobal, then the bottom proton becomes delocalized and bilobal, then the top proton becomes localized on its acceptor, and finally the bottom proton becomes localized on its acceptor. Note that this mechanism serves as an example of the type of behavior that can be captured with generalized NEO-MSDFT dynamics and may not occur in the experimentally relevant regime for this system.

We now present the results for the Ehrenfest trajectory of this double proton transfer process, as shown in Figure 5. The distances between the transferring protons and their donors and acceptors are shown in Figures 5A and 5B. The trajectory begins in the same manner as the adiabatic trajectory for the first $\sim$ 3 fs, at which point the quantum amplitudes of each adiabatic vibronic state begin to change (Figure 5C). Differences in the proton densities between the Ehrenfest and adiabatic trajectories are apparent even in this $\sim 3-4$ fs range. Most notably, the two protons do not appear to tunnel in an asynchronous manner as observed in the adiabatic trajectory. Instead, both protons start to delocalize at approximately the same time due to the mixing of the two adiabatic vibronic states in the total vibronic wave function (see the proton density at 3.85 fs in Figure 5E). At 4.15 fs, both protons are delocalized and bilobal, and the zwitterionic diabatic vibronic state begins to dominate the ground NEO-MSDFT adiabatic vibronic state. At this time, the first excited NEO-MSDFT adiabatic vibronic state begins to be weighted more heavily than the ground adiabatic vibronic state due to the large value of the nonadiabatic coupling in this region, and the zwitterionic diabatic vibronic state begins dominating the first excited adiabatic vibronic state as the system

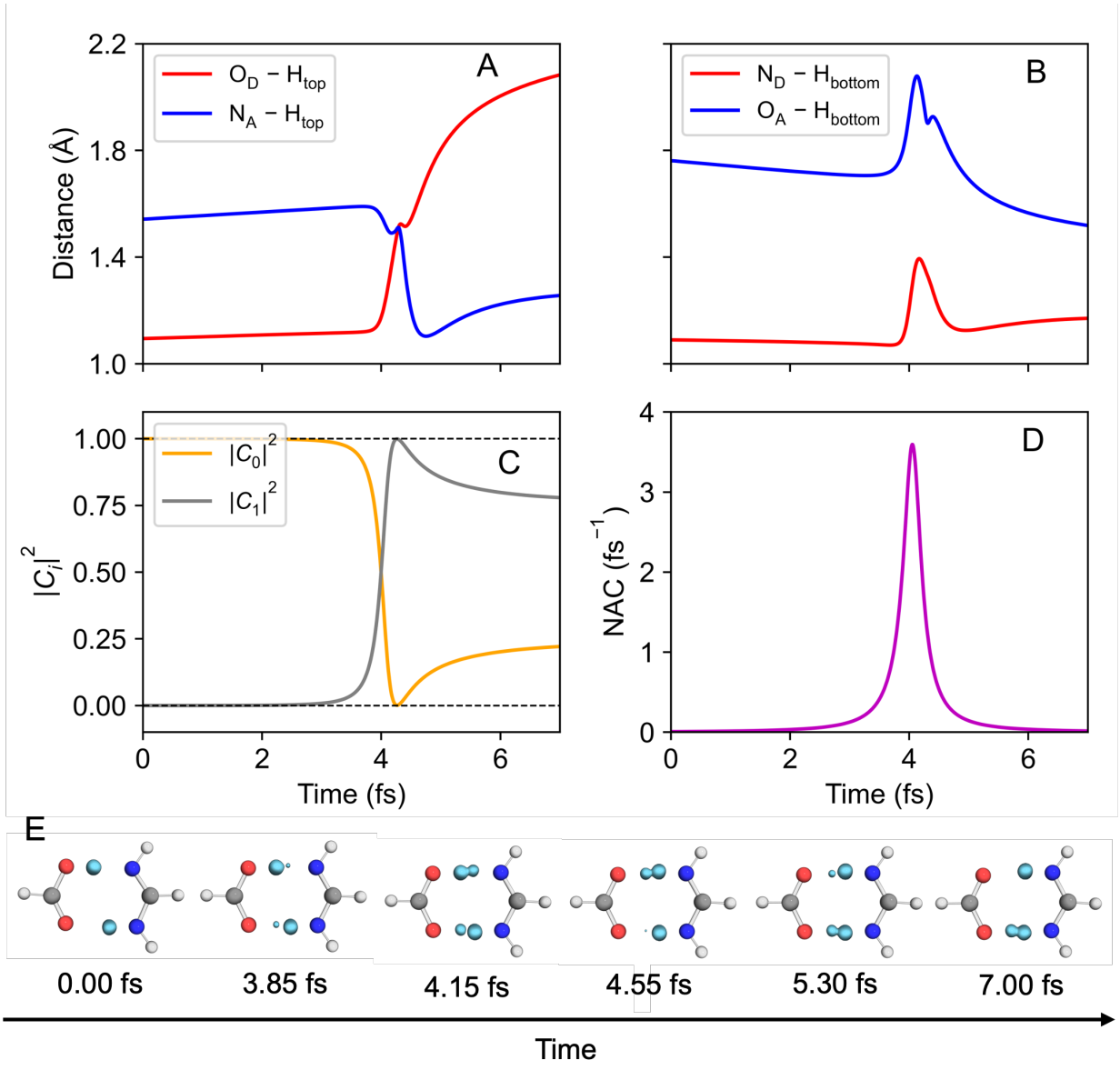

Figure 5. Analysis of the Ehrenfest trajectory for the FFAH. The distances between the (A) top and (B) bottom proton position expectation values and the corresponding donor (red) and acceptor (blue) for the average NEO-MSDFT vibronic state are plotted along the trajectory. (C) Quantum probabilities of the ground (orange) and first excited (gray) NEO-MSDFT adiabatic vibronic states. (D) Nonadiabatic coupling element between the ground and first excited NEO-MSDFT adiabatic vibronic states. (E) Proton density associated with the average NEO-MSDFT adiabatic vibronic state shown in cyan along the Ehrenfest trajectory.

exits this region of strong nonadiabatic coupling (Figure S4). This behavior causes the bottom proton to localize back to its initial position on its donor, while the top proton remains delocalized and bilobal (see the proton density at 4.55 fs in Figure 5E). When the top proton becomes localized on its acceptor, the bottom proton begins to delocalize again (see the proton density at 5.30 fs in Figure 5E), and the bottom proton does not complete its transfer over the course of this trajectory.

Thus, in the Ehrenfest trajectory, one proton transfer was inhibited, and the successful proton transfer was delayed compared to the adiabatic trajectory. We emphasize that the bottom proton is expected to localize on one side eventually due to thermal fluctuations. If the trajectory were propagated for a longer time, the proton would most likely localize near its acceptor. Moreover, another region of strong nonadiabatic coupling would eventually occur, leading to further nonadiabatic hydrogen tunneling dynamics. This short trajectory is simply an illustration of the type of tunneling dynamics that can be captured by the NEO-MSDFT Ehrenfest approach.

Next we propagated a sample surface hopping trajectory, as illustrated in Figure 6. The sample surface hopping trajectory proceeds in precisely the same manner as the adiabatic trajectory until 4.05 fs, when the nonadiabatic coupling reaches its maximum value (Figure 6D) and the transition to the first excited NEO-MSDFT adiabatic vibronic state was pre-determined to occur. Note that the top proton starts tunneling (i.e., becomes delocalized and bilobal) at $\sim$3.65 fs, as it did in the adiabatic trajectory, prior to the nonadiabatic transition. The system remains in the first excited NEO-MSDFT adiabatic vibronic state for 0.25 fs until a transition to the ground NEO-MSDFT adiabatic vibronic state occurs at 4.30 fs. Note that the bottom proton is predicted to start tunneling (i.e., become delocalized and bilobal) over this time range in the adiabatic trajectory. The bottom proton also starts tunneling over this time range in the sample surface hopping trajectory, even when the system is in the excited NEO-MSDFT adiabatic vibronic state. Thus, the proton densities and expectation values are similar for the sample surface hopping trajectory as for the adiabatic trajectory. Note that this single trajectory is not meaningful because surface hopping requires the propagation of many trajectories.

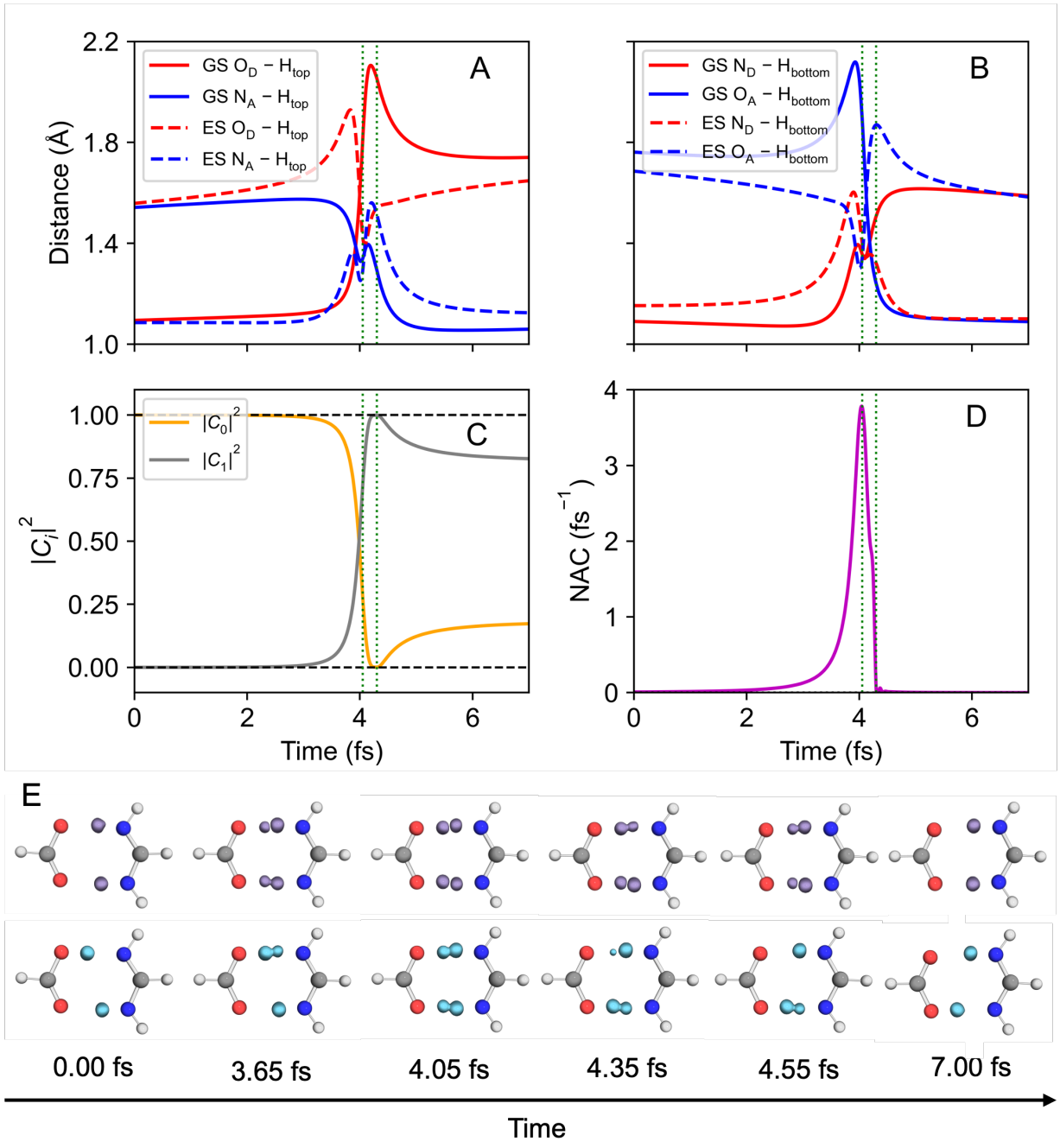

Figure 6. Analysis of the sample surface hopping trajectory for the FFAH. The distances between the (A) top and (B) bottom proton position expectation values and the corresponding donor (red) and acceptor (blue) for the ground (solid) and first excited (dashed) NEO-MSDFT adiabatic vibronic states are plotted along the trajectory. (C) Quantum probabilities of the ground (orange) and first excited (gray) NEO-MSDFT adiabatic vibronic states. (D) Nonadiabatic coupling element between the ground and first excited NEO-MSDFT adiabatic vibronic states. (E) Proton densities of the ground and first excited NEO-MSDFT adiabatic vibronic states shown in cyan and purple, respectively, along the sample surface hopping trajectory. The two vertical dotted green lines in (A-D) indicate where the two predetermined nonadiabatic transitions occurred along the trajectory. The system was in the first excited NEO-MSDFT adiabatic vibronic state for the time between these two dotted green lines.

5. Conclusions

In this work, we have introduced a scheme for obtaining the analytical gradients and nonadiabatic coupling vectors between NEO-MSDFT adiabatic vibronic states obtained using the generalized NEO-MSDFT method.[37] This scheme is amenable to an arbitrary number of localized NEO-DFT diabatic vibronic states, thus allowing for the simulation of multiple proton transfer processes. We applied this generalized gradient scheme to simulate the nonadiabatic hydrogen tunneling dynamics of the double proton transfer processes in the FAD and the FFAH systems. The application of the NEO-MSDFT method to the FAD requires only two diabatic vibronic states, corresponding to the reactant and product states, but the application to the FFAH requires the inclusion of a zwitterionic intermediate as well. We have shown that the generalized NEO-MSDFT approach can provide insight into the hydrogen tunneling dynamics of multiple proton transfer systems, properly accounting for the contribution of each localized diabatic vibronic state to the delocalized adiabatic vibronic states. The incorporation of nonadiabatic effects for these systems was found to slow down, or in some cases completely inhibit, these proton transfer processes.

A more quantitative picture of hydrogen tunneling dynamics comparable to experiment can be captured with NEO-MSDFT by sampling over initial conditions at finite temperature and running a large number of nonadiabatic dynamics trajectories. However, further refinement of the NEO-MSDFT method may be required to allow the proton basis function centers to move during the dynamics in a tractable manner. A more accurate description of hydrogen tunneling dynamics may also require a quantum mechanical treatment of the heavier nuclei of the system.[70] This work provides the foundation for simulating nonadiabatic hydrogen tunneling phenomena in a variety of systems, from individual proton transfer processes to proton relays, potentially in condensed phases using NEO hybrid quantum mechanical/molecular mechanical methods[24,71] or even electronically excited states.[34]

Supporting Information

NEO-MSDFT Hamiltonian and overlap matrix elements and their gradients; physical motivation for the form of the off-diagonal Hamiltonian matrix elements; derivatives related to generalized eigenvalue problems; nonadiabatic coupling terms between NEO-DFT diabatic states; expectation values for mixed NEO-MSDFT states; time-dependent nonadiabatic coupling elements; additional plots for all trajectories; analytical vs numerical gradients and nonadiabatic coupling vectors; energy conservation analysis; initial conditions for trajectories; Cartesian coordinates of relevant molecular geometries.

Acknowledgments

The authors thank Dr. Eno Paenurk and Dr. Scott Garner for helpful discussions and comments on the manuscript. The authors thank Dr. Chris Malbon, Dr. Jonathan Fetherolf, Dr. Chiara Donatella Aieta, Dr. Alexander Soudackov, Prof. Tao E. Li, Prof. Patrick H. Vaccaro, Mathew Chow, Millan Welman, Rachel Stein, and Rowan Goudy for useful discussions. This work was supported by the National Science Foundation Grant No. CHE-1954348, CHE-2415034, and CHE-2408934. J. A. D. was also supported by the National Institutes of Health Grant 1T32GM149438.

Data Availability Statement

The data that support the findings of this study are available within this article and its supplementary material. The code used to propagate the dynamics is available in GitHub at https://github.com/joseph-dickison20/namd/. The generalized NEO-MSDFT approach is available in Q-Chem 6.1.[61]

References

(1) Cha, Y.; Murray, C. J.; Klinman, J. P. Hydrogen Tunneling in Enzyme Reactions. *Science* **1989**, *243*, 1325.

(2) Richardson, J. O.; Pérez, C.; Lobsiger, S.; Reid, A. A.; Temelso, B.; Shields, G. C.; Kisiel, Z.;

Wales, D. J.; Pate, B. H.; Althorpe, S. C. Concerted Hydrogen-Bond Breaking by Quantum Tunneling in the Water Hexamer Prism. *Science* **2016**, *351*, 1310.

(3) Vaillant, C. L.; Wales, D. J.; Althorpe, S. C. Tunneling Splittings in Water Clusters from Path Integral Molecular Dynamics. *J. Phys. Chem. Lett.* **2019**, *10*, 7300.

(4) Litman, Y.; Richardson, J. O.; Kumagai, T.; Rossi, M. Elucidating the Nuclear Quantum Dynamics of Intramolecular Double Hydrogen Transfer in Porphycene. *J. Am. Chem. Soc.* **2019**, *141*, 2526.

(5) Hammarström, L.; Styring, S. Proton-Coupled Electron Transfer of Tyrosines in Photosystem II and Model Systems for Artificial Photosynthesis: The Role of a Redox-Active Link Between Catalyst and Photosensitizer. *Energy Environ. Sci.* **2011**, *4*, 2379.

(6) Stubbe, J.; Nocera, D. G.; Yee, C. S.; Chang, M. C. Y. Radical Initiation in the Class I Ribonucleotide Reductase: Long-Range Proton-Coupled Electron Transfer? *Chem. Rev.* **2003**, *103*, 2167.

(7) Hammes-Schiffer, S. Hydrogen Tunneling and Protein Motion in Enzyme Reactions. *Acc. Chem. Res.* **2006**, *39*, 93.

(8) Webb, S. P.; Iordanov, T.; Hammes-Schiffer, S. Multiconfigurational Nuclear-Electronic Orbital Approach: Incorporation of Nuclear Quantum Effects in Electronic Structure Calculations. *J. Chem. Phys.* **2002**, *117*, 4106.

(9) Pavošević, F.; Culpitt, T.; Hammes-Schiffer, S. Multicomponent Quantum Chemistry: Integrating Electronic and Nuclear Quantum Effects Via the Nuclear–Electronic Orbital Method. *Chem. Rev.* **2020**, *120*, 4222.

(10) Tao, Z.; Yu, Q.; Roy, S.; Hammes-Schiffer, S. Direct Dynamics with Nuclear–Electronic Orbital Density Functional Theory. *Acc. Chem. Res.* **2021**, *54*, 4131.

(11) Yu, Q.; Roy, S.; Hammes-Schiffer, S. Nonadiabatic Dynamics of Hydrogen Tunneling with Nuclear-Electronic Orbital Multistate Density Functional Theory. *J. Chem. Theory Comput.* **2022**, *18*, 7132.

(12) Pavošević, F.; Culpitt, T.; Hammes-Schiffer, S. Multicomponent Coupled Cluster Singles and Doubles Theory within the Nuclear-Electronic Orbital Framework. *J. Chem. Theory Comput.* **2019**, *15*, 338.

(13) Pavošević, F.; Rousseau, B. J. G.; Hammes-Schiffer, S. Multicomponent Orbital-Optimized Perturbation Theory Methods: Approaching Coupled Cluster Accuracy at Lower Cost. *J. Phys. Chem. Lett.* **2020**, *11*, 1578–1583.

(14) Pak, M. V.; Chakraborty, A.; Hammes-Schiffer, S. Density Functional Theory Treatment of Electron Correlation in the Nuclear–Electronic Orbital Approach. *J. Phys. Chem. A* **2007**, *111*, 4522.

(15) Brorsen, K. R.; Yang, Y.; Hammes-Schiffer, S. Multicomponent Density Functional Theory: Impact of Nuclear Quantum Effects on Proton Affinities and Geometries. *J. Phys. Chem. Lett.* **2017**, *8*, 3488.

(16) Yang, Y.; Brorsen, K. R.; Culpitt, T.; Pak, M. V.; Hammes-Schiffer, S. Development of a Practical Multicomponent Density Functional for Electron-Proton Correlation to Produce Accurate Proton Densities. *J. Chem. Phys.* **2017**, *147*, 114113.

(17) Yang, Y.; Culpitt, T.; Hammes-Schiffer, S. Multicomponent Time-Dependent Density Functional Theory: Proton and Electron Excitation Energies. *J. Phys. Chem. Lett.* **2018**, *9*, 1765.

(18) Zhao, L.; Tao, Z.; Pavošević, F.; Wildman, A.; Hammes-Schiffer, S.; Li, X. Real-Time Time-Dependent Nuclear-Electronic Orbital Approach: Dynamics Beyond the Born–Oppenheimer Approximation. *J. Phys. Chem. Lett.* **2020**, *11*, 4052–4058.

(19) Zhao, L.; Wildman, A.; Tao, Z.; Schneider, P.; Hammes-Schiffer, S.; Li, X. Nuclear–Electronic Orbital Ehrenfest Dynamics. *J. Chem. Phys.* **2020**, *153*, 224111.

(20) Zhao, L.; Wildman, A.; Pavošević, F.; Tully, J. C.; Hammes-Schiffer, S.; Li, X. Excited State Intramolecular Proton Transfer with Nuclear-Electronic Orbital Ehrenfest Dynamics. *J. Phys. Chem. Lett.* **2021**, *12*, 3497.

(21) Li, T. E.; Tao, Z.; Hammes-Schiffer, S. Semiclassical Real-Time Nuclear-Electronic Orbital Dynamics for Molecular Polaritons: Unified Theory of Electronic and Vibrational Strong Couplings. *J. Chem. Theory Comput.* **2022**, *18*, 2774–2784.

(22) Li, T. E.; Hammes-Schiffer, S. Nuclear-Electronic Orbital Quantum Dynamics of Plasmon-Driven H_2 Photodissociation. *J. Am. Chem. Soc.* **2023**, *145*, 18210–18214.

(23) Li, T. E.; Paenurk, E.; Hammes-Schiffer, S. Squeezed Protons and Infrared Plasmonic Resonance Energy Transfer. *J. Phys. Chem. Lett.* **2024**, *15*, 751–757.

(24) Chow, M.; Li, T. E.; Hammes-Schiffer, S. Nuclear–Electronic Orbital Quantum Mechanical/Molecular Mechanical Real-Time Dynamics. *J. Phys. Chem. Lett.* **2023**, *14*, 9556–9562.

(25) Hammer, T.; Coutinho-Neto, M. D.; Viel, A.; Manthe, U. Multiconfigurational Time-Dependent Hartree Calculations for Tunneling Splittings of Vibrational States: Theoretical Considerations and Application to Malonaldehyde. *J. Chem. Phys.* **2009**, *131*, 224109.

(26) Wang, Y.; Braams, B. J.; Bowman, J. M.; Carter, S.; Tew, D. P. Full-Dimensional Quantum Calculations of Ground-State Tunneling Splitting of Malonaldehyde Using an Accurate Ab Initio Potential Energy Surface. *J. Chem. Phys.* **2008**, *128*, 224314.

(27) Schröder, M.; Gatti, F.; Meyer, H.-D. Theoretical Studies of the Tunneling Splitting of Malonaldehyde Using the Multiconfiguration Time-Dependent Hartree Approach. *J. Chem. Phys.* **2011**, *134*, 234307.

(28) Pak, M. V.; Hammes-Schiffer, S. Electron-Proton Correlation for Hydrogen Tunneling Systems. *Phys. Rev. Lett.* **2004**, *92*, 103002.

(29) Pak, M. V.; Swalina, C.; Webb, S. P.; Hammes-Schiffer, S. Application of the Nuclear–Electronic Orbital Method to Hydrogen Transfer Systems: Multiple Centers and Multiconfigurational Wavefunctions. *Chem. Phys.* **2004**, *304*, 227–236.

(30) Yu, Q.; Hammes-Schiffer, S. Nuclear-Electronic Orbital Multistate Density Functional Theory. *J. Phys. Chem. Lett.* **2020**, *11*, 10106.

(31) Mo, Y.; Bao, P.; Gao, J. Energy Decomposition Analysis Based on a Block-Localized Wavefunction and Multistate Density Functional Theory. *Phys. Chem. Chem. Phys.* **2011**, *13*, 6760.

(32) Gao, J.; Grofe, A.; Ren, H.; Bao, P. Beyond Kohn–Sham Approximation: Hybrid Multistate Wave Function and Density Functional Theory. *J. Phys. Chem. Lett.* **2016**, *7*, 5143.

(33) Grofe, A.; Qu, Z.; Truhlar, D. G.; Li, H.; Gao, J. Diabatic-at-Construction (DAC) Method for Diabatic and Adiabatic Ground and Excited States Based on Multistate Density Functional Theory. *J. Chem. Theory Comput.* **2017**, *13*, 1176.

(34) Lu, Y.; Gao, J. Multistate Density Functional Theory of Excited States. *J. Phys. Chem. Lett.* **2022**, *13*, 7762.

(35) Skone, J. H.; Pak, M. V.; Hammes-Schiffer, S. Nuclear-Electronic Orbital Nonorthogonal Configuration Interaction Approach. *J. Chem. Phys.* **2005**, *123*, 134108.

(36) Thom, A. J. W.; Head-Gordon, M. Hartree–Fock Solutions as a Quasidiabatic Basis for Nonorthogonal Configuration Interaction. *J. Chem. Phys.* **2009**, *131*, 124113.

(37) Dickinson, J. A.; Yu, Q.; Hammes-Schiffer, S. Generalized Nuclear-Electronic Orbital Multistate Density Functional Theory for Multiple Proton Transfer Processes. *J. Phys. Chem. Lett.* **2023**, *14*, 6170–6178.

(38) Hammes-Schiffer, S.; Tully, J. C. Proton Transfer in Solution: Molecular Dynamics with Quantum Transitions. *J. Chem. Phys.* **1994**, *101*, 4657.

(39) Klein, S.; Bearpark, M. J.; Smith, B. R.; Robb, M. A.; Olivucci, M.; Bernardi, F. Mixed State 'On the Fly' Non-adiabatic Dynamics: The Role of the Conical Intersection Topology. *Chem. Phys. Lett.* **1998**, *292*, 259–266.

(40) Crespo-Otero, R.; Barbatti, M. Recent Advances and Perspectives on Nonadiabatic Mixed Quantum–Classical Dynamics. *Chem. Rev.* **2018**, *118*, 7026.

(41) Curchod, B. F. E.; Martínez, T. J. Ab Initio Nonadiabatic Quantum Molecular Dynamics. *Chem. Rev.* **2018**, *118*, 3305.

(42) Agostini, F.; Curchod, B. F. E. Different Flavors of Nonadiabatic Molecular Dynamics. *Wiley Interdiscip. Rev. Comput. Mol. Sci.* **2019**, *9*, 1417.

(43) Marsili, E.; Olivucci, M.; Lauvergnat, D.; Agostini, F. Quantum and Quantum-Classical Studies of the Photoisomerization of a Retinal Chromophore Model. *J. Chem. Theory Comput.* **2020**, *16*, 6032–6048.

(44) Siddique, F.; Barbatti, M.; Cui, Z.; Lischka, H.; Aquino, A. J. A. Nonadiabatic Dynamics of Charge-Transfer States Using the Anthracene–Tetracyanoethylene Complex as a Prototype. *J. Phys. Chem. A* **2020**, *124*, 3347–3357, Publisher: American Chemical Society.

(45) Li, X.; Tully, J. C.; Schlegel, H. B.; Frisch, M. J. Ab Initio Ehrenfest Dynamics. *J. Chem. Phys.* **2005**, *123*, 084106.

(46) Tully, J. C. Molecular Dynamics with Electronic Transitions. *J. Chem. Phys.* **1990**, *93*, 1061.

(47) Tully, J. C. Mixed Quantum-Classical Dynamics. *Faraday Discuss.* **1998**, *110*, 407.

(48) Yu, Q.; Schneider, P. E.; Hammes-Schiffer, S. Analytical Gradients for Nuclear–Electronic Orbital Multistate Density Functional Theory: Geometry Optimizations and Reaction Paths. *J. Chem. Phys.* **2022**, *156*, 114115.

(49) Mil'nikov, G. V.; Kühn, O.; Nakamura, H. Ground-State and Vibrationally Assisted Tunneling in the Formic Acid Dimer. *J. Chem. Phys.* **2005**, *123*, 074308.

(50) Barnes, G. L.; Squires, S. M.; Sibert, E. L. Symmetric Double Proton Tunneling in Formic Acid Dimer: A Diabatic Basis Approach. *J. Phys. Chem. B* **2008**, *112*, 595.

(51) Jain, A.; Sibert, E. L. Tunneling Splittings in Formic Acid Dimer: An Adiabatic Approximation to the Herring Formula. *J. Chem. Phys.* **2015**, *142*, 084115.

(52) Qu, C.; Bowman, J. An Ab Initio Potential Energy Surface for the Formic Acid Dimer: Zero-Point Energy, Selected Anharmonic Fundamental Energies, and Ground-State Tunneling Splitting Calculated in Relaxed 1–4-Mode Subspaces. *Phys. Chem. Chem. Phys.* **2016**, *18*, 24835.

(53) Richardson, J. O. Full- and Reduced-Dimensionality Instanton Calculations of the Tunnelling Splitting in the Formic Acid Dimer. *Phys. Chem. Chem. Phys.* **2017**, *19*, 966.

(54) Agranat, I.; Riggs, N. V.; Radom, L. The Formamidine–Formic Acid Dimer: a Theoretical Examination of its Equilibrium Structure and of the Double-Proton-Transfer Process. *J. Chem. Soc., Chem. Commun.* **1991**, 80–81.

(55) Lim, J.-H.; Lee, E. K.; Kim, Y. Theoretical Study for Solvent Effect on the Potential Energy Surface for the Double Proton Transfer in Formic Acid Dimer and Formamidine Dimer. *J. Phys. Chem. A* **1997**, *101*, 2233–2239.

(56) Kim, Y.; Lim, S.; Kim, Y. The Role of a Short and Strong Hydrogen Bond on the Double Proton Transfer in the Formamidine-Formic Acid Complex: Theoretical Studies in the Gas Phase and in Solution. *J. Phys. Chem. A* **1999**, *103*, 6632–6637.

(57) Cembran, A.; Song, L.; Mo, Y.; Gao, J. Block-Localized Density Functional Theory (BLDFT), Diabatic Coupling, and Their Use in Valence Bond Theory for Representing Reactive Potential Energy Surfaces. *J. Chem. Theory Comput.* **2009**, *5*, 2702.

(58) Fatehi, S.; Alguire, E.; Shao, Y.; Subotnik, J. E. Analytic Derivative Couplings Between Configuration-Interaction-Singles States with Built-In Electron-Translation Factors for Translational Invariance. *J. Chem. Phys.* **2011**, *135*, 234105.

(59) Fatehi, S.; Subotnik, J. E. Derivative Couplings with Built-In Electron-Translation Factors: Application to Benzene. *J. Phys. Chem. Lett.* **2012**, *3*, 2039–2043.

(60) Meek, G. A.; Levine, B. G. Evaluation of the Time-Derivative Coupling for Accurate Electronic State Transition Probabilities from Numerical Simulations. *J. Phys. Chem. Lett.* **2014**, *5*, 2351.

(61) Epifanovsky, E.; Gilbert, A. T. B.; Feng, X.; Lee, J.; Mao, Y.; Mardirossian, N.; Pokhilko, P.; White, A. F.; Coons, M. P.; Dempwolff, A. L.; Gan, Z. Software for the Frontiers of Quantum Chemistry: An Overview of Developments in the Q-Chem 5 Package. *J. Chem. Phys.* **2021**, *155*, 084801.

(62) Jain, A.; Alguire, E.; Subotnik, J. E. An Efficient, Augmented Surface Hopping Algorithm That Includes Decoherence for Use in Large-Scale Simulations. *J. Chem. Theory Comput.* **2016**, *12*, 5256–5268.

(63) Lee, C.; Yang, W.; Parr, R. G. Development of the Colle-Salvetti Correlation-Energy Formula into a Functional of the Electron Density. *Phys. Rev. B* **1988**, *37*, 785.

(64) Becke, A. D. Density-Functional Thermochemistry. III. The Role of Exact Exchange. *J. Chem. Phys.* **1993**, *98*, 5648.

(65) Dunning, T. H. Gaussian Basis Sets for Use in Correlated Molecular Calculations: 1. The Atoms Boron through Neon and Hydrogen. *J. Chem. Phys.* **1989**, *90*, 1007.

(66) Yu, Q.; Pavošević, F.; Hammes-Schiffer, S. Development of Nuclear Basis Sets for Multicomponent Quantum Chemistry Methods. *J. Chem. Phys.* **2020**, *152*, 244123.

(67) Liu, A.; Chow, M.; Wildman, A.; Frisch, M. J.; Hammes-Schiffer, S.; Li, X. Simultaneous Optimization of Nuclear–Electronic Orbitals. *J. Phys. Chem. A* **2022**, *126*, 7033–7039.

(68) Hasecke, L.; Mata, R. A. Nuclear Quantum Effects Made Accessible: Local Density Fitting in Multicomponent Methods. *J. Chem. Theory Comput.* **2023**, *19*, 8223–8233.

(69) Hasecke, L.; Mata, R. A. Optimization of Quantum Nuclei Positions with the Adaptive Nuclear-Electronic Orbital Approach. *J. Phys. Chem. A* **2024**, *128*, 3205–3211.

(70) Tuckerman, M. E.; Marx, D. Heavy-Atom Skeleton Quantization and Proton Tunneling in "Intermediate-Barrier" Hydrogen Bonds. *Phys. Rev. Lett.* **2001**, *86*, 4946.

(71) Chow, M.; Lambros, E.; Li, X.; Hammes-Schiffer, S. Nuclear–Electronic Orbital QM/MM Approach: Geometry Optimizations and Molecular Dynamics. *J. Chem. Theory Comput.* **2023**, *19*, 3839–3848.

TOC Graphic